Modeling the Asian Dust Aerosol Based on Ground Observations of Solar Radiation and Its Application to SeaWiFS

[1]B.J. Sohn, [2]H. Fukushima, [3]W. Takahashi, [4]T. Nakajima, [5]T. Murayama, [6]S. Ohta, [1]D.H. Kim, and [1]S.S. Lee

[1]Deparment of Earth Sciences, Seoul National University, Seoul, Korea
[2]School of High-Technology for Human Welfare, Tokai University, Numazu, Japan
[3]JAPAN NUS CO., LTD, Tokyo, Japan
[4]Center for Climate System Research, University of Tokyo, Tokyo, Japan
[5]Division of Physics, Tokyo University of Mercantile Marine, Tokyo, Japan
[6]Department of Sanitary and Environmental Engineering, Hokkaido University, Sapporo, Japan

1. INTRODUCTION

It has been known that the yellow sand (Asian dust) is heavy dust originated from the desert areas of North China and its significant portion is transported to the North Pacific Ocean (Uematsu et al., 1983). In particular, during the spring time, the yellow sand event results in poor visibility in East Asia. Many attempts have been made to examine the optical and chemical characteristics as well as long-range transport issues (Tanaka et al., 1989 among many others).

Here we provide some results of the aerosol optical characteristics from spectral extinction and diffuse sky radiation measurements near the Yellow Sea, in conjunction with visible radiation measurements by SeaWiFS ocean color sensor. Optical properties obtained by ground observations of solar radiation in this study can provide valuable information to the verification and development of satellite aerosol remote sensing as well as ocean color remote sensing.

2. GROUND MEASUREMENTS OF SOLAR RADIATION AND ANALYSIS

The direct and diffuse solar radiation measurements were carried out at the background atmosphere monitoring site (36.517°N, 126.317°E) in Anmyon Do which is located on the west coast of the Korean peninsula. Among the experiment data measured from 10 March 1998 to 15 August 1998, four days (March 16, 17, April 19, and 28) of measurements are analyzed in order to emphasize optical properties of yellow sand whose event took place on April 19 and 28. Other two days represent base aerosol.

2.1 Sun Photometer Data

Spectral direct solar irradiance has been measured using PREDE sun photometer (PSF-100) at four wavelengths λ=0.368. 0.500, 0.675, and 0.778 μm. The aerosol optical thickness $\tau_{a\lambda}$ has been determined by subtracting optical thickness by Rayleigh scattering ($\tau_{m\lambda}$) and by ozone absorption ($\tau_{o\lambda}$), i.e.:

$$\tau_{a\lambda} = \frac{\ln(F_{o\lambda}/F_{\lambda})}{m} - \tau_{m\lambda} - \tau_{o\lambda} \quad (1)$$

where $F_{o\lambda}$ is the direct solar radiation assumed to be at the top of the atmosphere and F_{λ} is the measured direct solar irradiance at the ground. Relative optical air mass m is obtained by the inverse of cosine of the solar zenith angle. Optical thickness by Rayleigh scattering is calculated using a formula by Hansen and Travis (1974), i.e.:

$\tau_{m\lambda} = (0.008569\ \lambda^{-4}\ (1+0.0113\ \lambda^{-2}+0.00013\ \lambda^{-4}))p/p_o$ (2)

where p is atmospheric surface pressure and p_o is the standard atmospheric pressure of 1013.25mb. For the calculation of ozone optical thickness, we use column ozone amount estimated by Nimbus 7 Total Ozone Mapping Spectrometer (TOMS).

2.2 Sky Radiometer Data

The PREDE sky radiometer (POM-01L) was used for measuring sky radiance in the solar aureole region at the wavelength of 315, 400, 500, 675, 870, 940, and 1020 nm. The solar aureole measurements were performed as follows: the sky radiances in the almucantar were measured every 20 min, starting from direct solar radiation, and then diffuse radiation with scattering angles from 0° to 60°.

The measured sky radiance data are analyzed by applying the inversion scheme developed by Nakajima et al. (1995) for the retrieval of optical thickness, volume spectra and phase function of the aerosol. The inversion method includes a radiative transfer algorithm to account for multiple scattering and it has been successfully used for various aerosol retrieval studies (Nakajima et al., 1995, Dalu et al., 1995). As inputs for the retrieval model, we used ground albedo of 0.1 and refractive index of 1.55-0.01*i* for the yellow sand and 1.50-0.01*i* for the base aerosol.

3. SEAWIFS DATA AND AEROSOL RETRIEVAL

The SeaWiFS is an ocean color sensor launched in 1997. It consists of 8 spectral bands; 412, 443, 490, 510, 555, 670, 765, and 865 nm. The last two near-infrared channels are used for determining atmospheric aerosol and then used for atmospheric correction. Nominal spatial resolution is about 1km at the nadir view. Detailed sensor characteristics are found in Gregg et al. (1994). In this research, we use global area coverage (GAC) data reduced from high resolution local area coverage (LAC) data generated by the scanner.

Analyses were performed for two cases of April 18 and 25, 1998, selected for contrasting the yellow sand aerosol with the background aerosol. The

atmospheric correction algorithm employed in the SeaWiFS data processing has two different aspects from CZCS algorithm, i.e.: to consider multiple scattering and to employ aerosol models. Since there is a near-linear relationship between aerosol multiple scattering and single scattering it is possible to calculate multiple scattering from single scattering effect with an aid of near-linear relationship between them (Gordon and Wang, 1994). SeaWiFS algorithm consists of 12 aerosol models, i.e.: oceanic models with relative humidity 90 and 99% of relative humidity, maritime models with 50, 70, 90 and 99%, coastal models with 50, 90 and 99%, and tropospheric models with 50 and 90% of relative humidity.

Because water leaving radiance in near IR region (765 and 865 nm in SeaWiFS channels) is nearly zero, we can compute aerosol single scattering effect by removing Rayleigh scattering, ozone absorption, and multiple scattering from the total reflectance. Aerosol contribution to the total radiance in the shorter wavelength region is computed by applying atmospheric correction parameter (ε) between two wavelengths, i.e.:

$$\varepsilon(\lambda_i,\lambda_j)=\frac{\rho_{as}(\lambda_i)}{\rho_{as}(\lambda_j)}=\frac{\omega_a(\lambda_i)\tau_a(\lambda_i)P_a(\theta,\theta_0,\lambda_i)}{\omega_a(\lambda_j)\tau_a(\lambda_j)P_a(\theta,\theta_0,\lambda_j)} \quad (3)$$

In Eq. (3), ω_a and P_a are single scattering albedo and phase function, and subscripts 'as' denotes aerosol single scattering. SeaWiFS algorithm first calculates the average of ε from 12 aerosol models between 765 and 865nm and selects two aerosol models holding nearest ε. Assuming in situ aerosol effect can be expressed by these two aerosol models, aerosol single scattering effect can be calculated.

4. RESULTS

4.1 Aerosol Optical Thickness

Aerosol optical thickness at 500 nm for the 4 observation days is presented in Fig. 1. Optical thickness is about 0.1 to 0.2 for clear days (March 16 and March 17). On both April 19 and 28, yellow sand aerosols are observed (Korean Meteorological Administration, 1998). It has been reported that heavy yellow sand event occurred from April 18 to 21 whereas mild yellow sand event is observed for a relatively short period in April 28. It is found that the optical thickness is dramatically increased during the heavy yellow sand event, reaching to the value around 0.9 that is much higher than the base value from 0.1 to 0.2. However, the increase of the aerosol optical thickness during weak yellow sand event (April 28) is moderate, showing around 0.3.

In order to examine the optical characteristics as a function of wavelength dependence of optical thickness we present the Ångström exponent (α)

$$\tau_{a\lambda}=\tau_{0.5}\left(\frac{\lambda}{0.5}\right)^{-\alpha} \quad (4)$$

where λ's are wavelengths of the sunphotometer. Here we use 500 and 778 nm for the calcuationof α. We show a scatter plot of $\tau_{0.5}$ versus α in Fig. 2. The Ångström exponent has a large variation from 0.2 to 1.2 in March 17. The large variation of the parameter may suggests a type of aerosol growth process due to the changes in relative humidity or in dust particles as noted in Nakajima et al. (1989). In the morning of March 17, dominant wind direction was easterly or north-easterly with which inland aerosol can be transported to the site. Major wind direction was changed into north-westerly in the afternoon so that marine type aerosol can be placed on the observation site. Besides relative humidity changes might contribute to the variations in Ångström exponent. By contrast, Ångström exponent is generally smaller for the yellow sand, in particular, heavy yellow sand event.

4.2 Aerosol Volume Spectrum

Fig. 3 shows the columnar aerosol volume spectra obtained from the sky radiation measurements. The assumed refractive index of aerosol is 1.55-0.01*i* for the yellow sand events independent of the wavelength. The obtained spectral distributions of base aerosol indicate a tri-modal pattern, showing modes at 0.08, 0.4, and 3 μm. The mode at 0.08 μm can be related to the background aerosol particles, and the mode at 0.4 μm and 3 μm of base aerosol can be related to sea salt particles since their sizes are those of typical maritime aerosols (d'Almeida et al., 1991). By contrast the spectra in the yellow sand events of 19 and 28 April, 1998 show significant increase of large particles ranging from 1 to 3 μm, with a new peak at around 2 μm. This peak around 2 μm found in the yellow sand cases is very consistent with the spectrum of near-ground aerosols measured from the Air-born Particle Counter (APC) at the same place -- see Fig. 4. Plots are drawn at the center diameter of 0.3-0.5, 0.5-0.82, 0.82-1.35, 1.35-2.23, 2.23-3.67, 3.67-6.06, 6.06-10, 10-25 μm from the left, thus the volume distribution shape in the ground sampler measurements matches to that obtained from sky radiation measurements.

4.3 Aerosol Phase Function

One of the important optical properties of aerosol is single scattering phase function. We retrieved aerosol phase function using Nakajima et al. (1995) retrieval algorithm. Considering that April 19 and 28 are days showing the yellow sand events, yellow sand can enhance scatterings throughout all angles, compared with phase functions of background aerosol of March 16 and 17 (not shown). Local minima are shown around 120° scattering angle. It is of interest that spectral dependence of the phase function is much weaker for yellow sand events (April 19, and 28).

4.4 Aerosol Characteristics Viewed from SeaWiFS Measurements

We calculated aerosol optical thickness at 765 and 865 nm. Aerosol optical thickness given in the

histogram as percentage area indicates that there are three dominant modes, 0.23, 0.4, and 0.8 of optical thickness. Latter two values are consistent with those in Fig. 1 for the yellow sand case. The value around 0.8 covers most of yellow sand area. Surrounding the yellow sand area is the second largest peak of aerosol optical thickness. From the trajectory analysis, it was found that weaker area of 0.4 was originated from the outer region of dust storm area in Mongolia. Therefore, the yellow sand area consists of two groups; an area showing optical thickness around 0.8 and the surrounding area with aerosol optical thickness around 0.4.

Fig. 6 shows scattergram of the aerosol optical thickness at 765 nm and the atmospheric correction parameter (ε) between 765 nm and 865 nm for April 18 and April 25. Striking difference is found in the features of scattering. In April 18, main values of ε are found between 1.05 and 1.15 widely varying with optical thickness from 0.2 and 0.85. The ε values smaller than 1.0 are considered to be cloud-contaminated pixels since they are mostly located in the cloud edge area. On the other hand, distributions in April 25 show wider variation of ε while optical thickness is much smaller and is confined around 0.2, comparing to the yellow sand case of April 18. This significantly different pattern of ε suggests that the yellow sand areas can be determined from SeaWiFS data by applying features obtained from atmospheric correction parameter and optical thickness.

5. REFERENCES

Dalu, G., R. Rao, A. Pompei, P. Boi, G. Tonna, and B. Olivieri, 1995: Aerosol optical properties retrieved from solar aureole measurements over southern Sardinia. *J. Geophys. Res.*, **100**, 26135-26140.

d'Almeida, G. A., P. Koepke, and E. P. Shettle, 1991: Atmospheric Aerosols: Global Climatotology and Radiative Characteristics. A. Deepak Publishing, 561pp.

Gregg, W.W., F.S. Patt, R.H. Woodward, 1994: The simulated SeaWiFS data set, Version 2. *NASA Technical Memorandum* 104566, Vol. 15, 42pp.

Gordon, H. R., and M. Wang, 1994: Retrieval of water-leaving radiance and aerosol optical thickness over the oceans with SeaWiFS : A preliminary algorithm, App. Opt., 33, 443-452

Hansen, J.E., and L.D. Travis, 1974: Light scattering in planetary atmospheres. *Space Science Reviews*, **16**, 527-610.

Fukushima, H., and J. Ishijaka, 1993: Special features and applications of CZCS data in Asian waters. *Ocean colour: Theory and applications in a decade of CZCS experience.* Ed. by V. Barale and P.M. Schlittenhardt, Kluwer Academic Publishers, 213-236.

Nakajima, T. et al., 1986: Consistency of aerosol size distributions inferred from measurements of solar radiation and aerosols. *J. Meteor. Soc. Japan*, **64** 765-776.

Nakajima, T. et al., 1989: Aerosol optical characteristics in the yellow sand events observed in May 1982 in Nagasaki -- Part II. Model. J. Meteor. Soc. Japan, 67, 279-291.

Nakajima, T. et al., 1995: Use of sky brightness measurements from ground for remote sensing of particulate polydispersions, *Applied Optics*, **35**, 2672-2686.

Tanaka, M., T. Nakajima, M. Shiobara, M. Yamano, and K. Arao, 1989: Aerosol optical characteristics in the yellow sand events observed in May, 1982 at Nagasaki - Part I Observations. *J. Meteor. Soc. Japan*, **67**, 267-278.

Uematsu, M., R. Duce, J.M. Prospero, L. Chen, and J.T. Merrill, and R.L. McDonald, 1983: Transport of mineral aerosol from Asia over the North Pacific ocean. *J. Geophys. Res.*, **88**, 5343-5352.

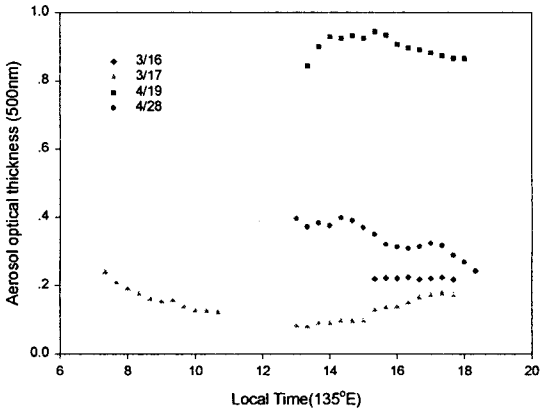

Fig. 1: Scatterplot of the instantaneous aerosol optical thickness at 500 nm.

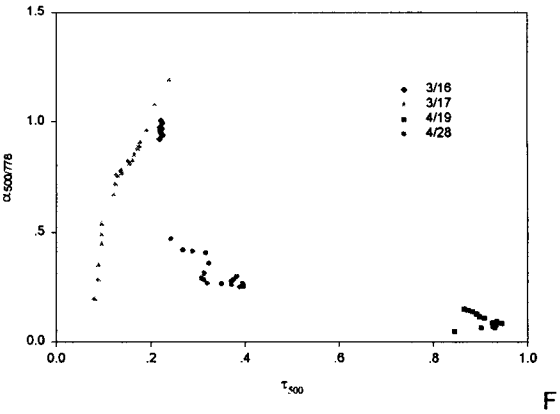

Fig. 2: Scatterplot of the Ångström exponent versus optical thickness.

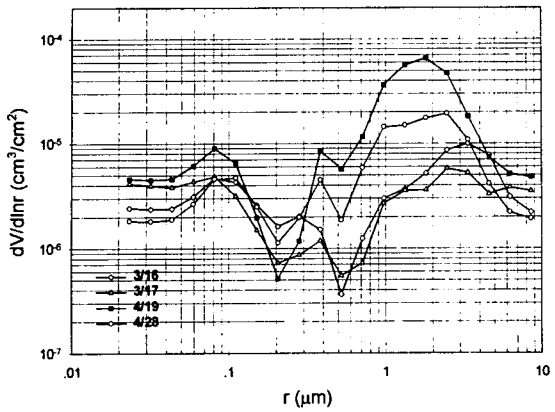

Fig. 3: Aerosol volume spectra. Cases of April 19 and April 28, 1998 correspond to the yellow sand events.

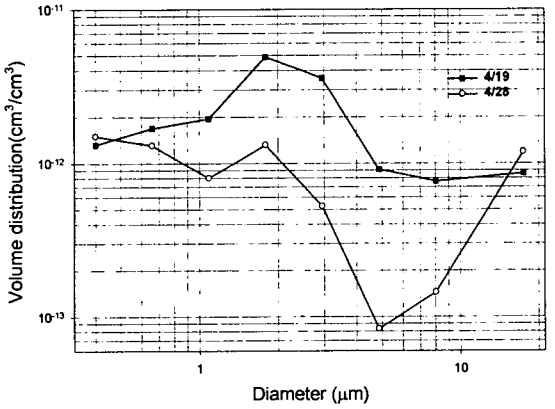

Fig. 4: Volume spectra of near-ground aerosols measured by the Air-born Particle Counter (APC) in April 19 and 28, 1998.

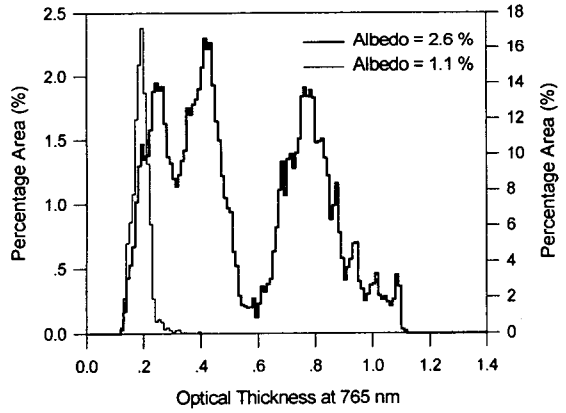

(a)

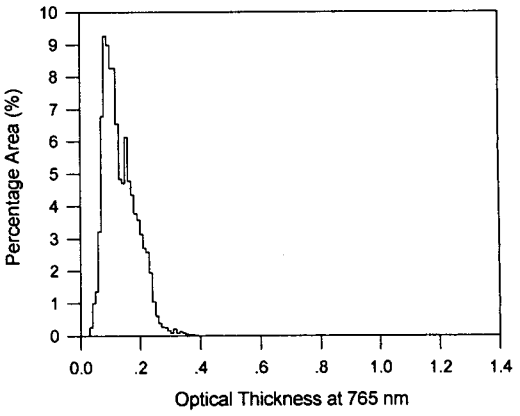

(b)

Fig. 5: Distributions of percentage area of aerosol optical thickness at 765 nm for (a) April 18, 1998, and (b) April 25, 1998. Note changed scale in the right ordinate of (a) for the original setting for the cloud threshold.

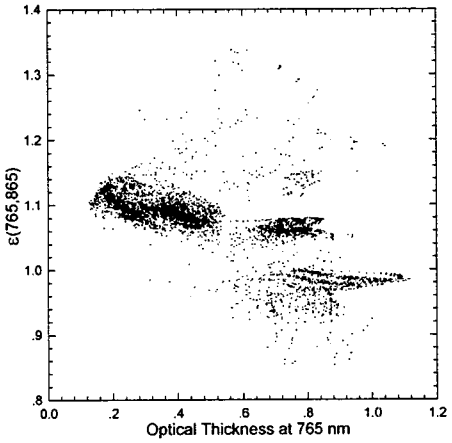

(a)

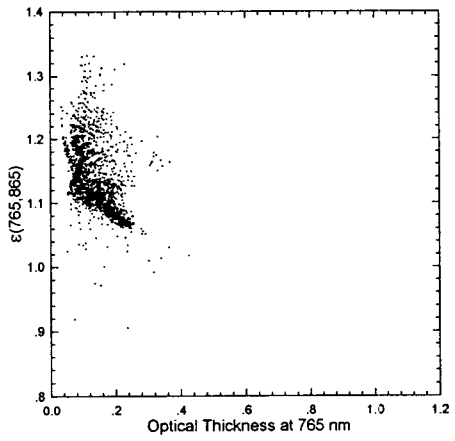

(b)

Fig. 6: Scattergram of atmospheric correction parameter (ε) and aerosol optical thickness for (a) April 18, 1998, and (b) April 25, 1998.